Distributed processing of movement signaling

Scott D. Kennedy[a,b,c] and Andrew B. Schwartz[a,b,c,1]

[a]Department of Bioengineering, University of Pittsburgh, Pittsburgh, PA 15260; [b]Center for the Neural Basis of Cognition, University of Pittsburgh and Carnegie Mellon University, Pittsburgh, PA 15261; and [c]Systems Neuroscience Center, University of Pittsburgh School of Medicine, Pittsburgh, PA 15213

Edited by Robert H. Wurtz, National Institutes of Health, Bethesda, MD, and approved October 18, 2019 (received for review September 13, 2019)

Basic neurophysiological research with monkeys has shown how neurons in the motor cortex have firing rates tuned to movement direction. This original finding would have been difficult to uncover without the use of a behaving primate paradigm in which subjects grasped a handle and moved purposefully to targets in different directions. Subsequent research, again using behaving primate models, extended these findings to continuous drawing and to arm and hand movements encompassing action across multiple joints. This research also led to robust extraction algorithms in which information from neuronal populations is used to decode movement intent. The ability to decode intended movement provided the foundation for neural prosthetics in which brain-controlled interfaces are used by paralyzed human subjects to control computer cursors or high-performance motorized prosthetic arms and hands. This translation of neurophysiological laboratory findings to therapy is a clear example of why using nonhuman primates for basic research is valuable for advancing treatment of neurological disorders. Recent research emphasizes the distribution of intention signaling through neuronal populations and shows how many movement parameters are encoded simultaneously. In addition to direction and velocity, the arm's impedance has now been found to be encoded as well. The ability to decode motion and force from neural populations will make it possible to extend neural prosthetic paradigms to precise interaction with objects, enabling paralyzed individuals to perform many tasks of daily living.

motor control | motor cortex | arm movement | kinematics | impedance

Neurons across many brain areas have firing rates that are modulated during physical interactions with the world. There is increasing evidence that the control mechanisms for movement are highly distributed throughout the nervous system. Neuroscientists have begun to use techniques that sample this widespread activity for brain-controlled interfaces that enable people who are paralyzed to move prosthetic limbs. These advances are based on studies in which monkeys made human-like movements, such as reaching, grasping, and even drawing. By combining "encoded" information from the firing rates of scores of neurons, investigators were able to construct extraction algorithms for "decoding" motion details from neural activity. Subsequently, these extraction algorithms were adapted so that a monkey's intention could be transformed to actual movement without a perceptible time lag, making it possible to operate a robotic arm and hand in real time. These studies formed the foundation for the use of brain-controlled interface technology by paralyzed human subjects, who have been able to control prosthetic limbs intuitively, with near-natural coordination and agility, to perform some tasks of daily living. Here, we review advances in brain-controlled interfaces for arm movement and discuss current efforts to establish control during hand–object interaction. Specifically, results are presented showing that context-dependent limb stiffness can be decoded from motor cortical activity, in much the same way that motion details were extracted in previous studies. These results, based on activity collected from populations of neurons, are further evidence of distributed processing in which multiple signals drive many individual neurons.

Decoding Movement Activity in the Motor Cortex

Arm-reaching paradigms with nonhuman primates have been used successfully over the last 40 y to develop population-based approaches for extracting detailed information related to the control of these volitional movements. In the primary motor cortex, as well as in other motor-related cortical regions, the firing rates of many neurons are modulated together as reaching takes place. A major factor driving the modulation of these rates is the direction of arm movement. In 1982, Apostolos Georgopoulos published his first paper (1) describing how motor cortical firing rates were modulated when monkeys made reaching movements in different directions (Fig. 1*A*). Monkeys performed a center-out task, by moving their hands from a center start position to 1 of 8 radially arranged targets. Since the targets were equally spaced around a circle, the movement directions were sampled uniformly, and these directions were the primary parameter that varied in the experiment. The firing rates of individual motor cortical neurons were recorded as the movements were made. By plotting the average firing rate during the movement against movement direction, each neuron's activity could be modeled as a cosine tuning function (Fig. 1*C*).

The equation that describes this cosine tuning is

$$FR = b_0 + b_x X + b_y Y, \quad [1]$$

where FR is the mean firing rate during the movement, averaged across trials to the same target. X and Y are the components of a unit vector pointing in the direction of movement. Multiple regression is used to find b_0, b_x, and b_y. The tuning function describes how movement direction is encoded in a single neuron's firing rate. The cosine function implies that a neuron has a "preferred direction," a combination of behavioral variables that corresponds to the maximal firing rate. In Fig. 1, these variables would be the x and y components of a vector that points to 90°. For movements away from the preferred direction, the neuron's firing rate decreases smoothly.

The tuning principle can be visualized in terms of 2 vectors, $\vec{M}$ for movement direction and $\vec{B}$ that points in the preferred direction of a neuron (Fig. 2). From Eq. **1**, $\vec{M}$ is composed of X and Y and $\vec{B}$

This paper results from the Arthur M. Sackler Colloquium of the National Academy of Sciences, "Using Monkey Models to Understand and Develop Treatments for Human Brain Disorders," held January 7–8, 2019, at the Arnold and Mabel Beckman Center of the National Academies of Sciences and Engineering in Irvine, CA. NAS colloquia began in 1991 and have been published in PNAS since 1995. From February 2001 through May 2019 colloquia were supported by a generous gift from The Dame Jillian and Dr. Arthur M. Sackler Foundation for the Arts, Sciences, & Humanities, in memory of Dame Sackler's husband, Arthur M. Sackler. The complete program and video recordings of most presentations are available on the NAS website at http://www.nasonline.org/using-monkey-models.

Author contributions: S.D.K. and A.B.S. designed research; S.D.K. performed research; S.D.K. and A.B.S. analyzed data; and A.B.S. wrote the paper.

The authors declare no competing interest.

This article is a PNAS Direct Submission.

Data deposition: The data used in Figs. 4–7 are available at https://knb.ecoinformatics.org/view/doi:10.5063/F14Q7SBK.

[1]To whom correspondence may be addressed. Email: abs21@pitt.edu.

First published December 23, 2019.

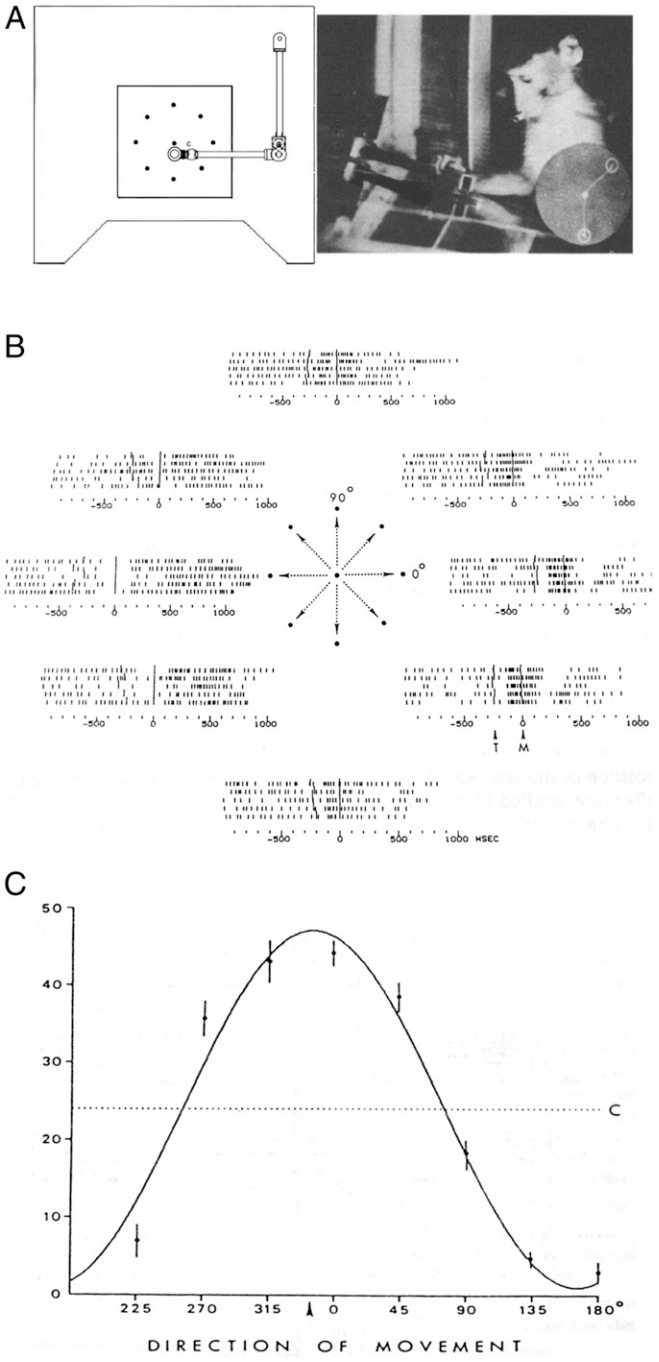

Fig. 1. Directional tuning. (*A*) Center-out task. Monkeys were trained to grasp the end of a manipulandum and capture a light embedded in the table top, by moving the site circle over the light. The task began by capturing the center light. This light was extinguished as 1 of 8 peripheral target positions was illuminated. The monkey had to quickly move and capture that light then hold still until a reward was administered. Reprinted with permission from ref. 59. (*B*) Unitary firing of motor cortical neurons was isolated with a single, moveable microelectrode. The firing of an example unit is displayed as rasters arranged in a circle corresponding to the direction the manipulandum was moved during the task. Each tick mark is placed at the time an action potential occurred during the trial (time = 0 was when the movement began; "T" is when the peripheral target appeared). There were 5 trials to each target, with firing rates during those trials represented on different lines of the rasters. Reprinted with permission from ref. 5. (*C*) Firing rates over the duration and across trials were averaged and plotted as a function of movement direction. Vertical bars are the SDs across trials. The data were fit with a cosine function having a preferred direction (direction with the highest firing rate) of ~0°. Reprinted with permission from ref. 5.

has components b_x and b_y. In a particular movement direction, the length of $\vec{B}$ (corresponding to the neuron's firing rate) will be proportional to the cosine of the angle between the neuron's preferred direction and the direction the arm is moving. A conceptual advantage of the vector cartoon is that, although the dimensions of the 2 vectors ($\vec{B}$ and $\vec{M}$ in Fig. 2) will increase with the number of modeled variables, the equation itself always has the same form. This feature has proven useful for extending the original 2-dimensional (2D) encoding models to 3 dimensions of arm movement, 3 dimensions of wrist movement, and 4 dimensions of hand shape (2–4), so that a total of 10 movement variables could be shown to be encoded in a single neuron's firing rate.

The vector concept is also useful for decoding neural activity. Decoding predicts movement direction from the observed firing rates. Note that decoding is the inverse of encoding, in which firing rates are predicted from movement. It might appear that decoding could be carried out with a single neuron if its tuning function was known. Decoding seemingly could be carried out by finding the movement direction on the tuning curve that matches the observed firing rate of the neuron. However, a single firing rate maps to 2 directions on the cosine function (except in the preferred direction). This redundancy, combined with the broad cosine tuning curve's being susceptible to large changes in direction for a small amount of noise in the firing rate, makes single-neuron decoding unfeasible. On the other hand, the broad tuning (the cosine covers the entire directional domain) means that every cosine-tuned neuron is encoding direction simultaneously. Therefore, a decoding process, based on a large sample of tuned neurons, can mitigate the redundancy and noise susceptibility problem of a single tuning function. A simple decoder—the "population vector algorithm"—provided a robust readout of movement direction from a sampled population of recorded single-unit activity (5). For each neuron in the population, a preferred direction was found and represented with a vector, $\vec{B}$ (Fig. 2). The mean firing rate of each unit during the movement was used to adjust the length of $\vec{B}$. Note that the cosine tuning model says that this firing rate is proportional to the $\cos\theta$, but for building the population vector, the actual firing rates are used. A sum of these contributions (one weighted $\vec{B}$ per neuron in the population) was taken, and the direction of the resultant population vector was found to point in the predicted direction of movement. Population vectors were built for each direction of movement in the center-out task.

Initially, the mean firing rate during each center-out movement trial was used both to calculate each neuron's preferred direction and to adjust the length of each contribution to the population vector. In later studies (6–10) the decoder was modified so that, although the mean rate was still used in the encoder to find each neuron's preferred direction, instantaneous firing calculated in bins of 10 to 20 ms was used in the decoder to extract direction. This modified algorithm resulted in a time series of population vectors during each trial. In addition to the vectors pointing in the direction of movement, it turned out that their lengths matched the time-varying speed of the hand during the task. When the vectors of the time series were connected tip to tail, the resulting path matched the actual trajectory of the arm. The emergence of speed from the population vector algorithm turned out to be due to the nonlinear encoding of speed and direction within single neurons (11, 12). Nevertheless, the emergence of speed from the decoder was fortuitous because it means that the population vector represents hand velocity; it predicts the instantaneous direction and speed of the hand so that the hand's trajectory can be predicted from neural activity. In practical terms, the population vectors can be used to show where the hand will be ~150 ms later. The arm's movement can be predicted continuously.

Trajectory prediction using the population vector algorithm was demonstrated with monkeys trained to trace different shapes

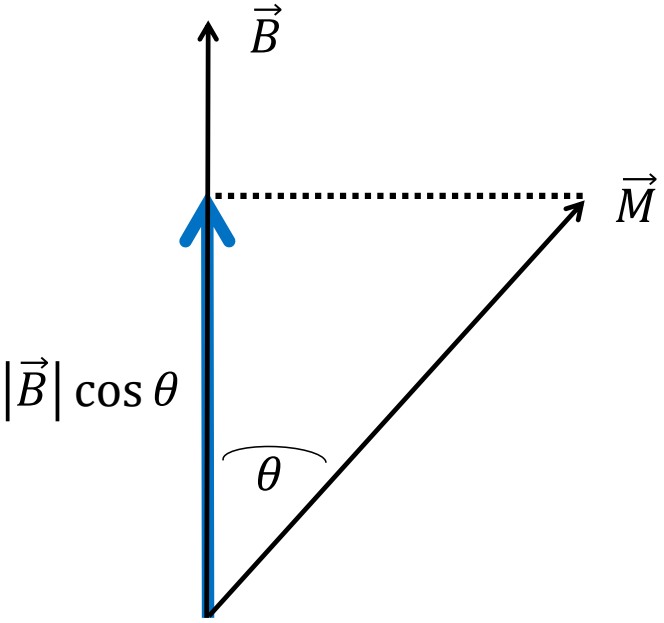

Fig. 2. Vector description of cosine tuning A vector, $\vec{B}$, points in the preferred direction and has a magnitude equal to the maximum firing rate of the neuron. $\vec{M}$ is a vector in the direction of arm movement with components of X and Y and a magnitude of 1. θ is the angle between the preferred direction and the direction of movement. A projection of $\vec{M}$ onto $\vec{B}$ shortens the length of $\vec{B}$ (superimposed blue vector), which now has a magnitude of $|\vec{B}|\cos\theta$. The length of the projection is proportional to the firing rate of the neuron when the arm moves at an angle θ from the preferred direction.

with their fingers. Monkeys repeatedly drew figures as different individual neural units were recorded. When enough data were collected, a time series of population vectors was calculated and used to construct predicted trajectories. These predictions closely matched the actual drawn figures (6–8, 10). In addition to recovering the shape of the figures, because velocity was extracted accurately, the psychophysical kinematic details of the movement could be recovered as well. These features, originally described from human drawing studies, included figural segmentation and the 2/3 power law (10). The extracted signal reflected high-level details consonant with natural features of behavior.

A number of laboratories in the late 1990s and early 2000s worked to develop brain-controlled interfaces in primates by decoding motor cortical activity. Some of these studies merely decoded ongoing arm movement (13, 14), while others used the recorded signals to move cursors in a computer display (15, 16). The essential elements used in this method were the use of chronically implanted, intracortical, microelectrode arrays and the ability to process the recorded signals quickly so that there was no noticeable lag between the subject's movement intention and the displayed movement. Our motivation at this time was to decode intended 3-dimensional (3D) arm movement as continuous trajectories. Population vector decoding was used to extract intended velocity to produce smooth, accurate, and robust trajectories (15). Monkeys with microwire electrode arrays implanted in their motor cortices were trained to move a cursor in a virtual-reality, 3D computer display to targets arranged to appear at the corners of a cube (3D center-out task). The task was first learned by monkeys moving their arms through space while viewing the virtual display, with the cursor locked to a marker on the hand. After the monkeys learned this "hand control" task, the motion of the cursor was unlinked from the hand marker and controlled by the real-time decoded brain signal ("brain control"). Since the movements were in 3D space, the tuning-equation vectors were now 3D, but otherwise the encoding and decoding operations were the same as in the 2D case. The monkeys readily learned this brain-control task and were able to move the cursor with nearly the same performance as that achieved with hand control.

In subsequent experiments, the brain-controlled interface experiment was elaborated by having monkeys use the decoded signal to move a robotic arm. In these and later experiments, we began using 96-site Utah electrode arrays (UEA) instead of microwire electrodes for chronic intracortical recording. Using 4-dimensional decoding (x-y-z position in space and opening and closing a pincer), monkeys were able to operate a robot to reach, grasp a piece of food, and bring it to their mouths in a self-feeding paradigm (17). Robotic performance was increased by adding a 3D wrist to the robot, increasing the decoding to 7 dimensions (x-y-z transport, yaw, pitch, and roll of the wrist, and open-closing of a hand), and requiring the monkey subjects to reach, orient, and close a robot hand on a cylindrical object (18). Ultimately, monkeys were trained to reach and grasp a large variety of objects while the velocities of their arms, hands, and fingers were tracked. Their hand shapes were described with 4 principal components. A tuning function composed of 10 factors (x-y-z transport, yaw, pitch, and roll of the wrist, and 4 hand shape factors) was used to build 10-dimensional population vectors which accurately represented all 10 simultaneous movement factors (3, 19).

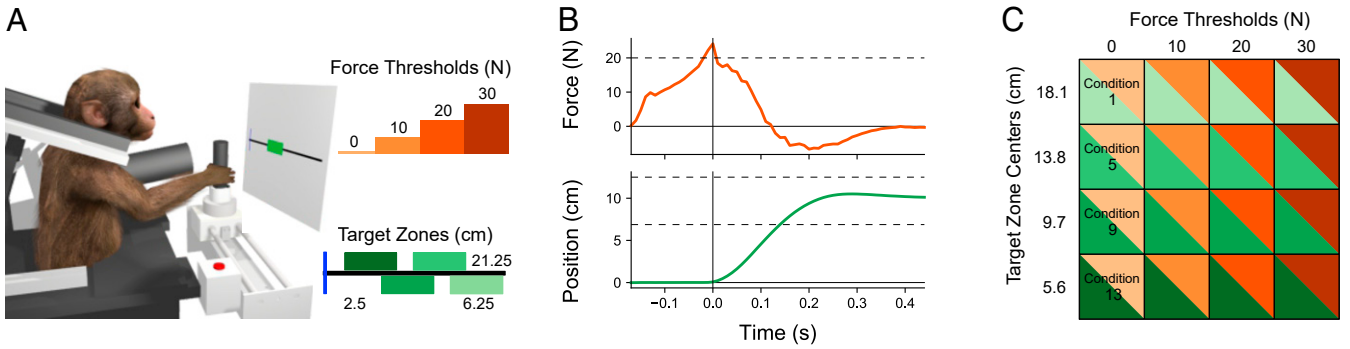

Fig. 3. Ballistic-release paradigm. (*A*) To initiate a trial, the monkey first pressed the start button (to the monkey's right) and then grasped the handle. The handle was pulled while it was locked in place until the force threshold was crossed. It was then unlocked to move freely along the track. To be successful, the monkey had to stop and hold the handle within the target zone for 300 ms. (*B*) Time plot of force and position a single trial. The vertical line at time 0 is when the handle was released. (*C*) Sixteen task conditions were composed of 4 force thresholds and 4 target zones.

Demonstrations in Human Subjects

Having demonstrated our ability to carry out the high-performance prosthetic control using a brain-controlled interface, we began an experiment with quadriplegic human subjects. The idea was for them to operate a prosthetic arm and hand to regain the functionality of their upper extremities lost to paralysis. In 2012, we began our experiment with Jan Scheuermann, who had been quadriplegic for 12 y. Two UEA microelectrode arrays were implanted in her left motor cortex. Thirteen weeks after the implantation, she was able to perform 7 degree-of-freedom (DOF) movements with the Modular Prosthetic Arm (20). This meant she was able to move a prosthetic hand to arbitrary positions in a 3D work space, orient the hand using a 3D wrist, and open and close the hand to grasp objects (21). In addition to spontaneous, intuitive reaching and grasping, Jan performed standardized reach-to-grasp exercises and showed steady improvement, so that these tasks were performed reliably with near-normal coordination. With additional training, she was able to add hand shaping to her repertoire, effectively controlling 10 DOF simultaneously (4).

In 2015, another quadriplegic participant, Nathan Copeland, was implanted with chronic microelectrode arrays. In addition to the 2 UEAs in his motor cortex for recording movement-related signaling, 2 additional arrays were placed in the hand area of his primary sensory motor cortex. These electrodes were used to elicit the sensation of pressure in his fingers, by passing microamp currents through the electrodes. The evoked sensations could be linked to pressure sensors in the fingertips of the prosthetic hand so that he can potentially "feel" the hand make contact with external objects (22).

These demonstrations showed that signals extracted with population decoding were robust enough to control many aspects of natural arm and hand movement. Over the last 20 y, a number of decoders based on large samples of single-unit firing rates have been developed. Most of those used in actual brain-controlled interface demonstrations have been "linear," in that they follow the general type of equation described in Eq. **1**, or make use of the cosine relation between movement direction and firing rate (15, 23–28). New decoders using machine-learning techniques may be useful when encoding models of neural activity are nonlinear (12, 29). Recent techniques based on neuron–neuron correlation may be especially promising because they extract latent input to a recorded population without relying on the presence of parameter tuning (30, 31). The new decoders, combined with new microelectrode recording technology, may dramatically increase the number of single units that can be recorded simultaneously (32–35). However, it should be noted that useful behaviors such as drinking with a straw have been demonstrated with as few as 2 or 3 DOF (36), showing that even a rudimentary control signal can be useful.

Our ultimate goal is to decode and generate a full repertoire of lost movement that is intuitive, with characteristics that match those produced naturally by subjects with intact motor abilities.

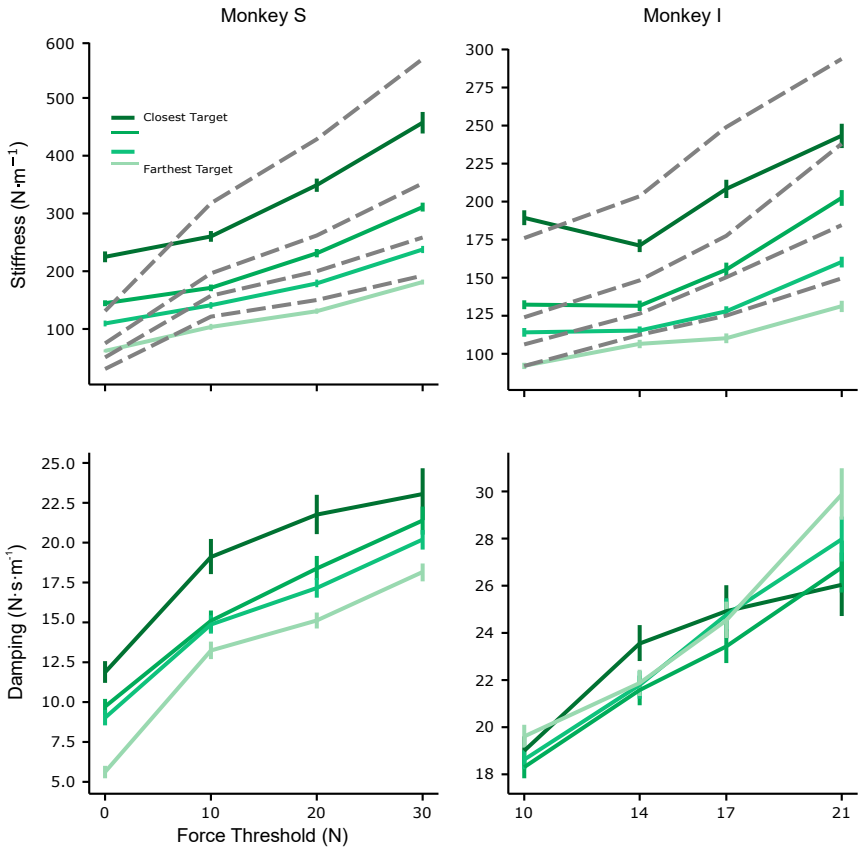

Fig. 4. Stiffness and damping. Both stiffness and damping covaried with both force threshold and target zone. The data were averaged across the 10 experimental sessions and across trials to the same combination of threshold and target zone. The mean values for each force–displacement combination are displayed with error bars indicating the 95% confidence interval. A dynamic physical model (solid lines) was fit using the force, displacement, and velocity that occurred in the 350 ms after the handle was released. Dashed lines in the stiffness figures were calculated as the ratio of force measured at handle release/ensuing displacement of the handle. For a given target zone, stiffness increased with force threshold. However, for target zones closer to the handle's lock position, the offset of the linear relation increased. There was clear separation of stiffness between conditions. Although damping also increased with force threshold, this was not as clear as the effect due to target distance. The overlap of the dashed and solid stiffness lines shows the 2 methods of calculating stiffness were equivalent.

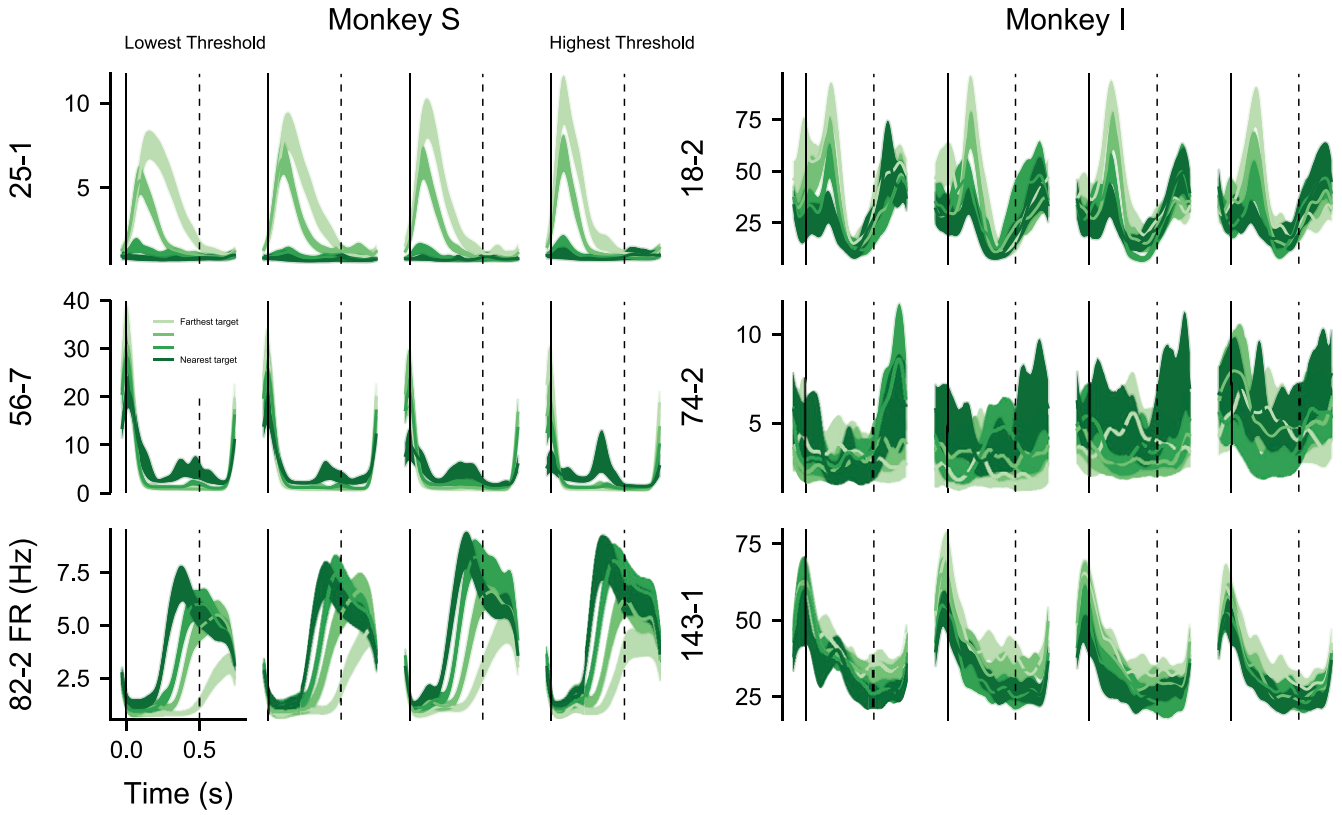

Fig. 5. Example firing rates units tended to be modulated with a general relation to motion (*Top*), force (*Middle*), or a combination of force and motion (*Bottom*). Shading represents the median and 95% confidence interval. Each response is labeled according to the recording channel and the sorted unit on that channel (channel-unit).

Accomplishment of this goal not only will require controlling the motion of the arm, hand, and fingers as they move through space but necessitates additional control of the arm and hand to contact and manipulate physical objects. This control encompasses tactile sensation and the precise regulation of force. Both of these are objectives of our current research program, as we describe in further detail later.

Decoding Impedance, or "Stiffness"

Most of the demonstrated tasks performed to date with brain-controlled interfaces relied almost entirely on the transport, orientation, and shaping of the hand taking place in free space. However, truly dexterous behavior requires the application of force in the correct amount, in the proper direction, and at specific locations on an object. The coordination of force and motion is captured in the mechanical parameter of impedance. Impedance can be thought of as the force resisting a displacement. When the hand is used to move an object, the moving object generates force back on the hand. Conversely, when force is applied to an object, that object will move in a particular manner. Prior knowledge of how an object will react to displacement and the application of force is a clear control requirement for action planning. This constraint has led to a movement control theory based on impedance (37). Impedance control is likely important for instances in which displacement and/or force changes so rapidly that feedback would be ineffective. As examples, consider what can happen at the onset of a reach when rapid movement of the arm is considered ballistic (38, 39) or upon initial contact of the hand with an object where large, rapid changes in force take place. In the latter situation, setting the impedance, or stiffness, of the hand before object contact could lead to effective displacement of the fingers and hand to help complete the task. Passive mechanics can be used as a means of control.

We used a ballistic-release task to determine whether a similar strategy—the presetting of mechanical impedance—could be used to control the arm when feedback of the movement would be ineffective. In an initial study (40), human subjects were seated in front of a computer monitor. They used their right arm to pull a handle along a horizontal track. The handle was locked in its start position with a strong magnet and released when 1 of 4 threshold forces was reached. Once released, the subjects were required to stop the handle in 1 of 4 position zones indicated on the computer monitor. Although the handle position and target zone were cued on the computer monitor, there was no display of force. A total of 16 force level/target position combinations were presented in blocks. This design was used to allow the subjects to anticipate a given combination. Repeats of release at the same force threshold and specified target distance made it possible for the subject to form an approximate prediction of the stiffness required for their arm to stop in the target zone. The idea was that subjects would cocontract their arm muscles to form a virtual spring. With the correct stiffness, their arm's motion would be arrested at the equilibrium position of this spring. This strategy would not require online feedback control and would be particularly effective in the fast transition following handle release.

This general idea, using antagonist muscles to form virtual springs about a joint, was proposed years ago by Anatol Feldman and was termed the "equilibrium-point hypothesis" (41, 42). Although this model may have limited, general applicability to arm movement (43), in special situations, such as ballistic-release, this type of strategy may be employed. Indeed, the results from our experiments with human subjects are consistent with this strategy.

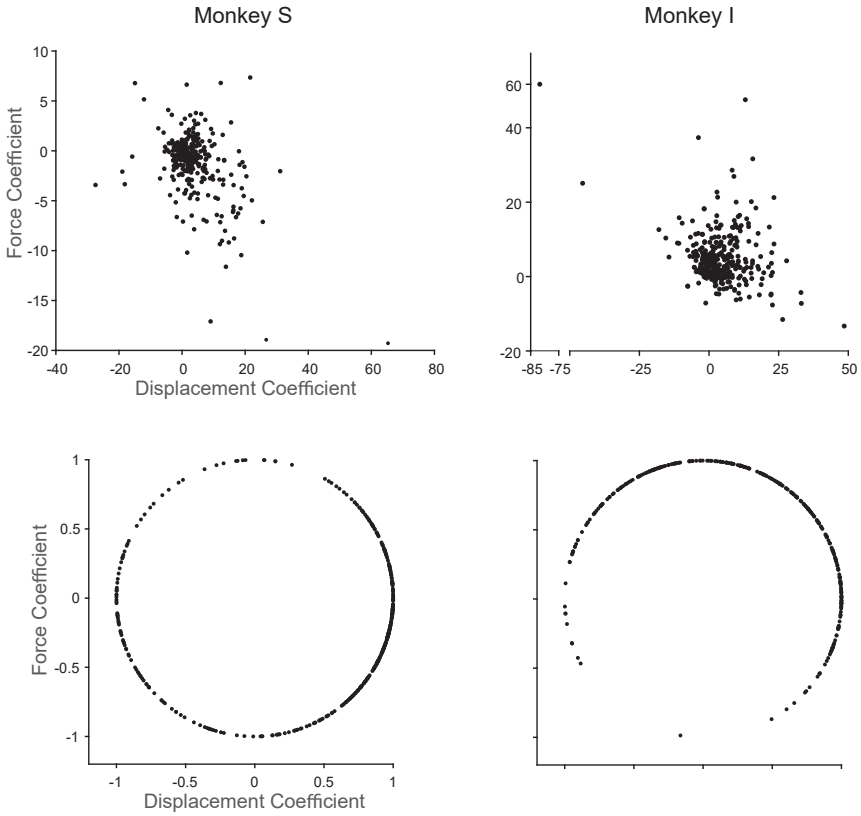

Fig. 6. Preferred directions. The regression coefficients, b_F and b_D, found using Eq. **2**, are displayed here as force and displacement coefficients for each of the tuned units across all experimental sessions. At the bottom the coefficients have been normalized to form a unit vector, $\left|\vec{B}\right| = 1$. The direction from the center of the circle corresponds to a preferred stiffness.

Coactivation of muscles that produced counteracting forces was found to be a major factor in setting this stiffness.

Having shown that human subjects adopted an impedance control strategy for the ballistic-release paradigm, we trained monkeys to perform the same task (Fig. 3). The experimental paradigms and use of nonhuman primates was thoroughly reviewed and approved by the Institutional Animal Care and Use Committee at the University of Pittsburgh. Once again the experimental design consisted of 16 combinations of 4 target zones and 4 force thresholds (Fig. 3*C*). Ten recording sessions were analyzed for each monkey.

Following the approach of the human experiments (40), 2 different calculations were used to find stiffness. In the first method, stiffness and damping were calculated using a physical dynamical model with the parameters of time-varying force, displacement, and velocity in the 350 ms following handle release. This was a measurement of the stiffness after the handle was released. In the second method stiffness was calculated at the instant of handle release, simply as the ratio of force produced by the subject to release the handle to the distance the handle was moved. The results of these 2 methods are plotted in the panels at the top of Fig. 4. Note that the stiffness traces are clearly separable by the 16 conditions. Furthermore, the 2 stiffness calculations gave consistent values across the data (compare the solid to the dashed stiffness traces). This finding suggests that stiffness at the beginning of the movement was essentially the same as that during the movement. This, and the finding that stiffness varied by task condition, shows that an impedance control strategy was used. The animals adapted the same strategy as human subjects: They adjusted the stiffness of their arms so that when the handle was released suddenly it would stop at the specified distance.

Motor cortical single-unit activity was recorded from 2 monkeys using UEAs (Blackrock Microsystems) on the precentral gyrus and Matrix (NeuroNexus) probes in the anterior bank of the central sulcus. Muscle activity (electromyography) was collected using epimysial electrodes chronically implanted on 15 arm and hand muscles (monkey S) or with surface recordings of 16 muscles (monkey I). Neural analysis was used to determine whether stiffness was encoded in the activity of motor cortical neurons and whether this could be decoded to extract stiffness from this brain structure.

An average of 105 single units from monkey S and 42 from monkey I were recorded simultaneously during each recording session. A total of 213 different units from monkey S and 101 from monkey I were recorded over the 10 complete sessions. Firing rates were calculated in 10-ms time bins aligned to the handle release, smoothed using a 30-ms Gaussian filter, and trial-averaged for each of the 16 behavioral conditions. Firing rate histograms from 6 example units are shown in Fig. 5. Many of the units had task-related patterns of modulation.

In order to determine whether stiffness was represented in the firing rates of these units with a relation that is similar to that found for kinematics, we tested a cosine tuning function of the form used in Eq. **1**:

$$FR = b_0 + b_F F + b_D D. \quad [2]$$

For this experiment, F is the force exerted to release the handle, D is the distance the hand traveled (the position value 630 ms after handle release), and FR is the mean firing rate over the first 600 ms of each trial, averaged across trials of the same condition. Tuning was assessed by fitting the regression model (Eq. **2**) to combinations of the force and displacement for each trial. The

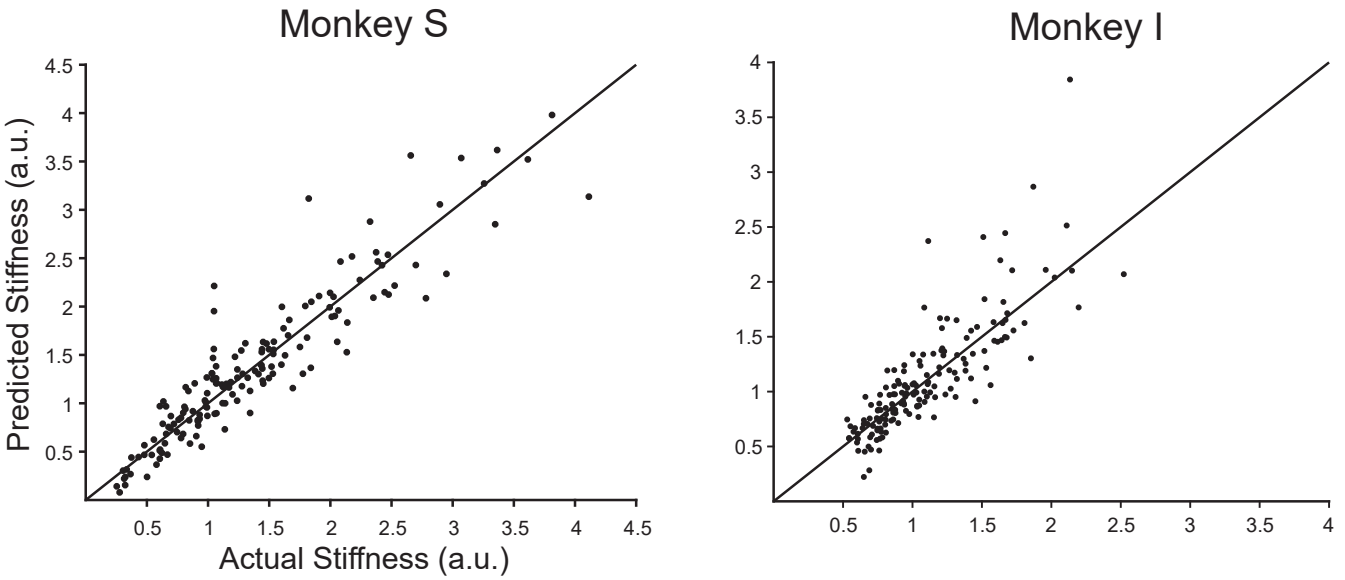

Fig. 7. Extracted stiffness tuned neurons recorded simultaneously in a single recording session were used in an OLE stiffness extraction algorithm to create population vectors. The population vectors had dimensions of force and displacement. Predicted stiffness was taken as the ratio of these dimensions, force–displacement. Results from all 10 sessions are shown for each monkey. The overall correlation coefficient of the combined data set for monkey S was $r = 0.89$ and for monkey I, $r = 0.83$. The solid line is actual = predicted stiffness.

force and displacement data were scaled so the 16 values of each ranged between 0 and 1. Using the vector formulation of this equation (Fig. 2), the preferred direction, $\vec{B}$, with components of b_F and b_D, corresponds to a vector pointing to the preferred stiffness. $\vec{M}$ has components of force and displacement instead of X and Y. The number of tuned neurons over the 10 experimental sessions for each monkey ranged from 32 to 54 for monkey S and from 21 to 48 for monkey I. For a neuron's response to be considered tuned, $R^2 > 0.1$ (goodness of fit from Eq. **2**) and $b_F > 0.01$. The regression coefficients from the tuned units are displayed in the top panel of Fig. 6. The directions of the preferred direction vectors, $\vec{B} = b_F b_D$, for each monkey are displayed in the bottom panel of Fig. 6. In this model, the preferred direction of each neuron's response is $\tan^{-1}\vec{B} = b_F/b_D$ and can be considered its "preferred stiffness." There was a bias along the displacement axis for monkey S, while for monkey I the distribution was biased in the positive force direction.

For each experimental session, the tuned units were used to build population vectors. The population vectors were calculated using optimal linear estimation (OLE) (25, 26). These vectors have 2 dimensions, force and displacement, and their ratio is the predicted stiffness extracted from the recorded population. Results collated across all 10 experimental sessions are shown in Fig. 7. Across individual sessions, the correlation coefficients for monkey S ranged from 0.87 to 0.98 and for monkey I from 0.71 to 0.93. These results show that stiffness can be extracted accurately from a population of motor cortical units using the same methodology for extracting arm velocity (44).

Discussion

The functional and anatomical components as well as the upper-limb capabilities of monkeys have a close correspondence to those of humans and this has motivated many motor control experiments. The study of how motor cortical activity is related to arm movement began with the development of the behaving monkey paradigm in the 1960s (45). These initial experiments were restricted to single-joint movement. With the introduction of less-restricted, whole-arm movement (1), it has become clear that motor cortical firing rates are modulated in association with multiple movement parameters (46–50). This multiplexing is a cardinal feature of distributed systems, with parameter representation dispersed over a large number of elements (51). Individual parameters may vary in their representation strength within a single neuron's firing rate, but even weak effects on firing rate can be decoded if they occur across a large number of neurons. Population algorithms capable of extracting these encoded parameters are now being used in brain-controlled interface paradigms to provide robust control of prosthetic devices. The control signal used for this neural prosthetic paradigm, although robust and accurate, has been limited to kinematic parameters governing the velocity of the arm, orientation of the hand, and shaping of the fingers (4). In order to extend this paradigm to practical interactions with everyday objects, both the force exerted on those objects and their displacement must be controlled simultaneously.

Impedance control theory (52) provides a biologically plausible framework in which force and displacement signals are generated in parallel. Impedance signaling can be used to control the force applied to an object when there is displacement of the hand and/or object taking place as contact between the two occurs. Importantly, the mechanical impedance of the hand allows it to yield to the near-instantaneous changes in object–hand force taking place upon initial contact. Feedback-dependent systems, especially those used in robots, often cannot respond quickly enough when actuators collide with an object, which can lead to an array of problems (53, 54). Biological systems with adjustable mechanical impedance, such as that afforded by muscle coactivation, make it possible for mechanical impedance to play a role in achieving a desired action goal. For instance, by presetting the impedance of the hand and fingers, the hand may quickly conform to the shape of an object upon initial contact. Similarly, proper mechanical impedance is essential for agile in-hand manipulation. To achieve this type of prosthetic control using brain-controlled interfaces, extracting impedance signals will be essential.

As an initial study of impedance signaling, we used a ballistic-release paradigm that encouraged subjects to set the muscle activity of their arms so that when moved suddenly, they would act as virtual springs, set with an impedance to arrest the arm in a target zone. After showing that human subjects used this spring strategy, monkeys performed the same task. Motor cortical activity was then fit with a cosine tuning function for stiffness.

Much of the unitary activity could be fit with this model, showing that stiffness was indeed encoded in motor cortical activity. This activity, when decoded with a population extraction algorithm, was shown to faithfully represent the stiffness used across experimental conditions to achieve the task.

The behaving primate model has allowed us to develop algorithms to extract detailed movement parameters. We have not yet fully described the functional mechanisms that the motor system uses to transform and transmit the information acting as input to the motor cortex, nor is it yet clear how the firing rates of these neurons act to effect movement. Nonetheless, recognition of these movement parameters helps to formulate overall control theories of how our motor system allows us to perform the elaborate manipulation of objects that is characteristic of human behavior. The strategy of using the behaving primate model to elucidate basic science correlates of volitional action has been, and will continue to be, essential for developing brain-based therapies for movement disorders. Furthermore, as we continue to investigate the mechanisms for planning and control of active manipulation, results from this research can provide a rigorous framework for the study of cognitive functioning (55–58), with the prospect of greater insight into high-order human thought and action.

The data used in Figs. 4–7 are available at https://knb.ecoinformatics.org/view/doi:10.5063/F14Q7SBK.

1. A. P. Georgopoulos, J. F. Kalaska, R. Caminiti, J. T. Massey, On the relations between the direction of two-dimensional arm movements and cell discharge in primate motor cortex. *J. Neurosci.* **2**, 1527–1537 (1982).
2. L. Castellanos, V. Q. Vu, S. Perel, A. B. Schwartz, R. E. Kass, A multivariate Gaussian process factor model for hand shape during reach-to-grasp movements. *Stat. Sin.* **25**, 5–24 (2015).
3. M. C. Spalding, "Characterizing the correlation between motor cortical neuronal firing and grasping kinematics," PhD dissertation, University of Pittsburgh, Pittsburgh, PA (2010).
4. B. Wodlinger *et al*., Ten-dimensional anthropomorphic arm control in a human brain-machine interface: Difficulties, solutions, and limitations. *J. Neural Eng.* **12**, 016011 (2015).
5. A. P. Georgopoulos, J. F. Kalaska, M. D. Crutcher, R. Caminiti, J. T. Massey, "The representation of movement direction in the motor cortex: Single cell and population studies" in *Dynamic Aspects of Neocortical Function*, G. M. Edelman, W. E. Goll, W. M. Cowan, Eds. (Neurosciences Research Foundation, Inc., 1984), pp. 501–524.
6. A. B. Schwartz, Direct cortical representation of drawing. *Science* **265**, 540–542 (1994).
7. D. W. Moran, A. B. Schwartz, Motor cortical activity during drawing movements: Population representation during spiral tracing. *J. Neurophysiol.* **82**, 2693–2704 (1999).
8. A. B. Schwartz, Motor cortical activity during drawing movements: Population representation during sinusoid tracing. *J. Neurophysiol.* **70**, 28–36 (1993).
9. A. P. Georgopoulos, R. E. Kettner, A. B. Schwartz, Primate motor cortex and free arm movements to visual targets in three-dimensional space. II. Coding of the direction of movement by a neuronal population. *J. Neurosci.* **8**, 2928–2937 (1988).
10. A. B. Schwartz, D. W. Moran, Motor cortical activity during drawing movements: Population representation during lemniscate tracing. *J. Neurophysiol.* **82**, 2705–2718 (1999).
11. D. W. Moran, A. B. Schwartz, Motor cortical representation of speed and direction during reaching. *J. Neurophysiol.* **82**, 2676–2692 (1999).
12. Y. Inoue, H. Mao, S. B. Suway, J. Orellana, A. B. Schwartz, Decoding arm speed during reaching. *Nat. Commun.* **9**, 5243 (2018).
13. R. E. Isaacs, D. J. Weber, A. B. Schwartz, Work toward real-time control of a cortical neural prothesis. *IEEE Trans. Rehabil. Eng.* **8**, 196–198 (2000).
14. J. Wessberg *et al*., Real-time prediction of hand trajectory by ensembles of cortical neurons in primates. *Nature* **408**, 361–365 (2000).
15. D. M. Taylor, S. I. Helms Tillery, A. B. Schwartz, Direct cortical control of 3D neuroprosthetic devices. *Science* **296**, 1829–1832 (2002).
16. M. D. Serruya, N. G. Hatsopoulos, L. Paninski, M. R. Fellows, J. P. Donoghue, Instant neural control of a movement signal. *Nature* **416**, 141–142 (2002).
17. M. Velliste, S. Perel, M. C. Spalding, A. S. Whitford, A. B. Schwartz, Cortical control of a prosthetic arm for self-feeding. *Nature* **453**, 1098–1101 (2008).
18. S. T. Clanton *et al*., "Seven degree of freedom cortical control of a robotic arm" in *Brain-Computer Interface Research*, C. Guger, B. Allison, G. Edlinger, Eds. (SpringerBriefs in Electrical and Computer Engineering, Springer, Berlin, 2013), pp. 73–81.
19. S. T. Clanton, "Brain-computer interface control of an anthropomorphic robotic arm," PhD thesis, Carnegie Mellon University, Pittsburgh, PA (2011).
20. M. Johannes *et al*., An overview of the developmental process for the modular prosthetic limb. *Johns Hopkins APL Tech. Dig.* **30**, 207–216 (2011).
21. J. L. Collinger *et al*., High-performance neuroprosthetic control by an individual with tetraplegia. *Lancet* **38**, 557–564 (2012).
22. S. N. Flesher *et al*., Intracortical microstimulation of human somatosensory cortex. *Sci. Transl. Med.* **8**, 361ra141 (2016).
23. W. Wu, Y. Gao, E. Bienenstock, J. P. Donoghue, M. J. Black, Bayesian population decoding of motor cortical activity using a Kalman filter. *Neural Comput.* **18**, 80–118 (2006).
24. V. Lawhern, W. Wu, N. Hatsopoulos, L. Paninski, Population decoding of motor cortical activity using a generalized linear model with hidden states. *J. Neurosci. Methods* **189**, 267–280 (2010).
25. Y. Zhang, S. M. Chase, Recasting brain-machine interface design from a physical control system perspective. *J. Comput. Neurosci.* **39**, 107–118 (2015).
26. E. Salinas, L. F. Abbott, Vector reconstruction from firing rates. *J. Comput. Neurosci.* **1**, 89–107 (1994).
27. S. Koyama *et al*., Comparison of brain-computer interface decoding algorithms in open-loop and closed-loop control. *J. Comput. Neurosci.* **29**, 73–87 (2010).
28. G. Santhanam, S. I. Ryu, B. M. Yu, A. Afshar, K. V. Shenoy, A high-performance brain-computer interface. *Nature* **442**, 195–198 (2006).
29. M. Burrow, J. Dugger, D. Humphrey, "Cortical control of a robot using a time-delay neural network" in *Proceedings of the International Conference on Rehabilitation Robotics* (Bath Institute of Medical Engineering, Bath, UK, 1997).
30. S. M. Chase, A. B. Schwartz, R. E. Kass, Latent inputs improve estimates of neural encoding in motor cortex. *J. Neurosci.* **30**, 13873–13882 (2010).
31. J. P. Cunningham, B. M. Yu, Dimensionality reduction for large-scale neural recordings. *Nat. Neurosci.* **17**, 1500–1509 (2014).
32. N. A. Steinmetz, C. Koch, K. D. Harris, M. Carandini, Challenges and opportunities for large-scale electrophysiology with Neuropixels probes. *Curr. Opin. Neurobiol.* **50**, 92–100 (2018).
33. R. M. Neely, D. K. Piech, S. R. Santacruz, M. M. Maharbiz, J. M. Carmena, Recent advances in neural dust: Towards a neural interface platform. *Curr. Opin. Neurobiol.* **50**, 64–71 (2018).
34. G. N. Angotzi *et al*., SiNAPS: An implantable active pixel sensor CMOS-probe for simultaneous large-scale neural recordings. *Biosens. Bioelectron.* **126**, 355–364 (2019).
35. E. Musk, An integrated brain-machine interface platform with thousands of channels. bioRxiv:10.1101/703801 (2 August 2019).
36. L. R. Hochberg *et al*., Reach and grasp by people with tetraplegia using a neurally controlled robotic arm. *Nature* **485**, 372–375 (2012).
37. N. Hogan, "Impedance control: An approach to manipulation" in *IEEE American Control Conference* (IEEE, 1984), pp. 304–313.
38. D. E. Meyer, J. E. K. Smith, C. E. Wright, Models for the speed and accuracy of aimed movement. *Psychol. Rev.* **89**, 449–482 (1982).
39. M. Desmurget, S. Grafton, "Feedback or feedforward control: End of a dichotomy" in *Taking Action: Cognitive Neuroscience Perspective on Intentional Acts*, S. H. Johnson-Frey, Ed. (MIT Press, 2003), pp. 289–338.
40. S. D. Kennedy, A. B. Schwartz, Stiffness as a control factor for object manipulation. *J. Neurophysiol.* **122**, 707–720 (2019).
41. A. G. Feldman, Change of muscle length as a consequence of a shift in the equibrium of muscle-load system. *Biophysics* **19**, 544–548 (1974).
42. A. G. Feldman, Once more on the equilibrium-point hypothesis (lambda model) for motor control. *J. Mot. Behav.* **18**, 17–54 (1986).
43. E. Bizzi, N. Accornero, W. Chapple, N. Hogan, Posture control and trajectory formation during arm movement. *J. Neurosci.* **4**, 2738–2744 (1984).
44. A. Schwartz, Distributed processing of movement signaling. Knowledge Network for Biocomplexity. http://doi.org/10.5063/F14Q7SBK. Deposited 11 October 2019.
45. E. V. Evarts, "Methods for recording activity of individual neurons in moving animals" in *Methods in Medical Research*, R. F. Rushmer, Ed. (Year Book Medical Publishers, 1966), pp. 241–250.
46. M. Omrani, M. T. Kaufman, N. G. Hatsopoulos, P. D. Cheney, Perspectives on classical controversies about the motor cortex. *J. Neurophysiol.* **118**, 1828–1848 (2017).
47. J. A. Pruszynski, J. Zylberberg, The language of the brain: Real-world neural population codes. *Curr. Opin. Neurobiol.* **58**, 30–36 (2019).
48. S. Saxena, J. P. Cunningham, Towards the neural population doctrine. *Curr. Opin. Neurobiol.* **55**, 103–111 (2019).
49. J. F. Kalaska, Emerging ideas and tools to study the emergent properties of the cortical neural circuits for voluntary motor control in non-human primates. *F1000 Res.* **8**, F1000 (2019).
50. A. B. Schwartz, Movement: How the brain communicates with the world. *Cell* **164**, 1122–1135 (2016).
51. G. M. Edelman, V. B. Mountcastle, *The Mindful Brain* (MIT Press, 1978).
52. N. Hogan, An organizing principle for a class of voluntary movements. *J. Neurosci.* **4**, 2745–2754 (1984).
53. N. Hogan, S. P. Buerger, "Impdedance and interaction control" in *Robotics and Automation Handbook*, T. R. Kurfess, Ed. (CRC Press, 2005), p. 24.
54. T. Morita, S. Sugano, "Design and development of a new robot joint using a mechanical impedance adjuster" in *Proceedings of 1995 IEEE International Conference on Robotics and Automation* (IEEE, 1995), pp. 2469–2475.
55. P. F. Dominey *et al*., "Implications of action-oriented paradigm shifts in cognitive neuroscience" in *The Pragmatic Turn. Toward Action-Oriented Views in Cognitive Neuroscience*, A. K. Engel, K. J. Friston, D. Kragic, Eds. (MIT Press, 2015), pp. 333–356.
56. R. Sanz, J. Gomez, C. Hernandez, I. Alarcon, "Thinking with the body: Towards hierarchical, scalable cognition" in *Handbook of Cognitive Science: An Embodied Approach*, P. Calvo, A. Gomila, Eds. (Elsevier, 2008), pp. 395–421.
57. S. H. Creem-Regehr, B. R. Kunz, Perception and action. *Wiley Interdiscip. Rev. Cogn. Sci.* **1**, 800–810 (2010).
58. R. A. Brooks *et al*., "Alternative essences of intelligence" in *Proceedings of the Fifteenth National/Tenth Conference on Artificial Intelligence/Innovative Applications of Artificial Intelligence* (American Association for Artificial Intelligence, Menlo Park, CA, 1998), pp. 961–968.
59. A. P. Georgopoulos, J. F. Kalaska, J. T. Massey, Spatial trajectories and reaction times of aimed movements: effects of practice, uncertainty, and change in target location. *J. Neurophysiol.* **46** (4) (1981).